RSC Advances

PAPER

View Article Online
View Journal | View Issue

Cite this: *RSC Adv.*, 2019, **9**, 39589

New red-emitting phosphor $Rb_xK_{3-x}SiF_7:Mn^{4+}$ (x = 0, 1, 2, 3): DFT predictions and synthesis†

Seunghun Jang,‡[a] June Kyu Park,‡[a] Minseuk Kim,[b] Kee-Sun Sohn,[b] Chang Hae Kim*[a] and Hyunju Chang*[a]

Received 31st July 2019
Accepted 19th November 2019

DOI: 10.1039/c9ra05929f

rsc.li/rsc-advances

Finding new phosphors through an efficient method is important in terms of saving time and cost related to the development of phosphor materials. The ability to identify new phosphors through preliminary simulations by calculations prior to the actual synthesis of the materials can maximize the efficiency of novel phosphor development. In this paper, we demonstrate the use of density functional theory (DFT) calculations to guide the development of a new red phosphor. We performed first-principles calculations based on DFT for pristine and Mn-doped $Rb_xK_{3-x}SiF_7$ (x = 0, 1, 2, 3) and predicted their stability, electronic structure, and luminescence properties. On the basis of the results, we then synthesized the stable $Rb_2KSiF_7:Mn^{4+}$ red conversion phosphor and investigated its luminescence, structure, and stability. As a result, we confirmed that $Rb_2KSiF_7:Mn^{4+}$ emitted red light with a longer wavelength than that emitted by $K_3SiF_7:Mn^{4+}$ and a wavelength similar to that of $K_2SiF_6:Mn^{4+}$. These results show that DFT calculations can provide rational insights into the design of a phosphor material before it is synthesized, thereby reducing the time and cost required to develop new red conversion phosphors.

1. Introduction

White-light-emitting diodes (WLEDs), which have been highlighted as next-generation light sources, have been widely studied because of their outstanding features, which include high durability, high energy conversion efficiency, low power consumption, and environmental friendliness.[1–3] To obtain white light, the strong blue-light emission from an InGaN light-emitting diode (LED) chip must be converted by color-conversion phosphor materials. Among numerous available conversion phosphors, an excellent red phosphor that exhibits a good color-rendering index is needed for WLEDs. Conventionally, $CaAlSiN_3:Eu^{2+}$ (CASN:Eu^{2+}) and $K_2SiF_6:Mn^{4+}$ are the representative red conversion phosphors with superior performance.[4–7] Because of their extensive color gamut and better color-rendering index, these phosphors have been widely used. In addition, a novel red narrow-band phosphor, $K_3SiF_7:Mn^{4+}$, with fluorescence characteristics similar to those of the $K_2SiF_6:Mn^{4+}$ phosphor has recently been introduced.[8] Although some progress has been made in terms of enhancing the feasibility of its synthesis and improving its decay time, the $K_3SiF_7:Mn^{4+}$ phosphor has a shortcoming in that the wavelength of its main photoluminescence (PL) peak is shorter than that of $K_2SiF_6:Mn^{4+}$, which inhibits its color-rendering index or reduces its color gamut.

To address this problem, we considered substituting the K^+ ions in $K_3SiF_7:Mn^{4+}$ with Rb^+ ions. When Rb^+, which is a member of the same periodic group as K^+ but has a larger atomic radius, is substituted for K^+ in the $K_3SiF_7:Mn^{4+}$ system, expansion of the lattice is expected. Such a change in the lattice is reasonably presumed to affect the luminescent properties of the system.

Meanwhile, theoretical approaches for the design of new phosphors can offer more effective ways to explore new conversion phosphor materials.[5,9] In our previous work, on the basis of first-principles studies based on density functional theory (DFT), we proposed that Sn- or Bi-doped CASN would be an effective alternative to Eu-doped CASN phosphors. Following our theoretical study, Sn- and Bi-doped CASN red phosphors were successfully prepared and their phosphor properties were experimentally demonstrated.[5,10]

In the present work, we performed first-principles calculations based on DFT for pristine and Mn-doped $Rb_xK_{3-x}SiF_7$ (x = 0, 1, 2, 3) and predicted their stability, electronic structure, and luminescence properties. In addition, on the basis of the knowledge gained from first-principles calculations, we synthesized $Rb_2KSiF_7:Mn^{4+}$ as a stable red conversion phosphor

[a]*Korea Research Institute of Chemical Technology, 141 Gajeong-ro, Yuseong-gu, Daejeon 34114, Republic of Korea*

[b]*Faculty of Nanotechnology and Advanced Materials Engineering, Sejong University, Seoul 05006, Republic of Korea. E-mail: changhae@krict.re.kr; hjchang@krict.re.kr; Fax: +82 42 860 7508; Tel: +82 42 860 7364*

† Electronic supplementary information (ESI) available: Atomic geometries for RbK_2SiF_7 and Rb_2KSiF_7, band structures and density of states (DOS) for $Rb_xK_{3-x}SiF_7$ structures, atomic and orbital projected DOSs of Rb_3SiF_7, atomic projected DOS on the ground and excited states of $Rb_xK_{3-x}SiF_7:Mn^{4+}$ structures. See DOI: 10.1039/c9ra05929f

‡ S. J. and J. K. P. contributed equally to this work.

and verified its PL properties, structure, and stability. The Rb_2KSiF_7:Mn^{4+} emitted red light with a wavelength longer than that of the red light emitted by K_3SiF_7:Mn^{4+} and similar to that of the light emitted by K_2SiF_6:Mn^{4+}. These results also show good agreement with the theoretical calculation results that indicated that the simulated emission wavelength of Rb_2KSiF_7:Mn^{4+} is the longest among the investigated phosphors. These results demonstrate that DFT calculations can provide rational insights into the properties of a phosphor material before it is synthesized, thereby reducing the time required to develop new red conversion phosphors.

2. Computational and experimental details

2.1. DFT calculations

The atomic and electronic structures of the $Rb_xK_{3-x}SiF_7$ ($x = 0$, 1, 2, 3) host materials were examined using the Vienna *ab initio* simulation package (VASP).[11,12] The exchange–correlation functional was approximated using the Perdew–Burke–Ernzerhof (PBE) expression.[13] The electron–ion interactions were modeled using the projector-augmented wave (PAW) method.[14] The electronic wave functions were expanded in a basis set of plane waves using a kinetic energy cutoff of 500 eV. Geometry relaxation steps were performed under the criterion that ionic forces were reduced to less than 0.01 eV $Å^{-1}$.

Mn-doped $Rb_xK_{3-x}SiF_7$ systems with Mn atoms substituted at Si sites were analyzed using a $1 \times 1 \times 2$ supercell structure. To optimize the geometry of each modeled structure, the *k*-space integration steps for pristine and Mn-doped $Rb_xK_{3-x}SiF_7$ structures were performed with finite sampling of the *k*-points on $7 \times 7 \times 9$ and $7 \times 7 \times 5$ meshes in the Brillouin zone, respectively. For the calculations of electronic structures, such as density of states (DOS) and band-structure calculations, the *k*-space integration steps for the pure and Mn-doped $Rb_xK_{3-x}SiF_7$ structures were performed with finite sampling of the *k*-points on $9 \times 9 \times 11$ and $9 \times 9 \times 7$ meshes in the Brillouin zone, respectively.

2.2. Synthesis

The novel red phosphor Rb_2KSiF_7:Mn^{4+} was successfully synthesized at room temperature *via* a two-step procedure, as shown in Fig. 1(a) and (b). Step 1 is the preparation of Rb_2SiF_6:Mn^{4+}; step 2 is sintering and washing to obtain the novel red phosphor Rb_2KSiF_7:Mn^{4+}.

A schematic of the liquid-state reaction (LSR) method is shown in Fig. 1(a). The raw materials used in the synthesis were Rb_2SiF_6 (Fluka, 99.0%), KF (Acros, 99%), $KMnO_4$ (Junsei Chemical Co., Ltd., 99.3%), KHF_2 (Sigma-Aldrich, 99%), HF (Avantor, 48%), H_2SiF_6 (SAMCHUN, 40%), and H_2O_2 (SAMCHUN, 34.5%). All chemical reagents were used as obtained without further purification. The overall synthesis process was conducted in a safe environment.

2.2.1. Procedure for synthesizing Mn^{4+}-activator, K_2MnF_6 (step 1 in Fig. 1). First, we synthesized Mn^{4+}-activator, K_2MnF_6 according to the following chemical reaction:

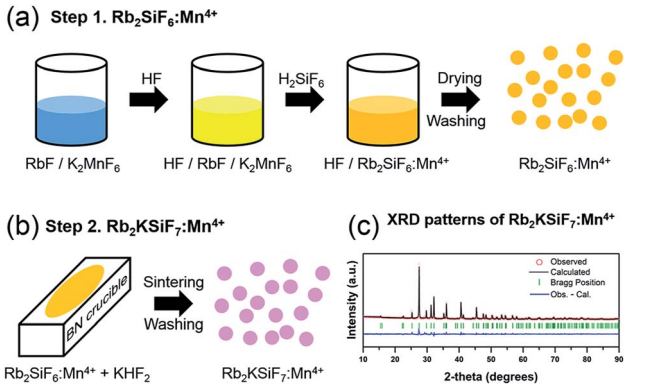

Fig. 1 Overall experimental procedure for the synthesis of the novel red phosphor Rb_2KSiF_7:Mn^{4+}: (a) procedure for the synthesis of Rb_2SiF_6:Mn^{4+} and (b) procedure for conversion from Rb_2SiF_6:Mn^{4+} to Rb_2KSiF_7:Mn^{4+}. (c) XRD pattern of the Rb_2KSiF_7:Mn^{4+} with its corresponding Rietveld refinement (solid line) and residual (observed–calculated).

$$2KMnO_4(s) + 2KF(s) + 10HF(aq) + 3H_2O_2 \rightarrow 2K_2MnF_6(s) + 8H_2O(l) + 3O_2(g)$$

KF and $KMnO_4$ powders were weighed in the appropriate quantitative stoichiometric ratio using a balance. The weighed powders were placed in a Teflon beaker, and the HF was added. The resultant mixture was stirred for approximately 1 h until the powders had completely dissolved. The color of the mixed solution immediately turned purple upon addition of the HF. H_2O_2 solution was then added dropwise to the reaction solution, which induced precipitation. The precipitated powder was then collected by filtration through filter paper. The obtained solid was dried in an oven for a specific time, resulting in K_2MnF_6 powder as an intermediate product.

2.2.2. Procedure for synthesizing Rb_2SiF_6:Mn^{4+} (step 1 in Fig. 1). Weighed powders of KF and K_2MnF_6 were placed in a Teflon beaker, and HF was added; the resultant mixture was stirred for several hours. The powder dissolved immediately and turned orange. A certain amount of H_2SiF_6 solution was added using a metering pump. The solution was stirred for few additional minutes, and an orange precipitate (Rb_2SiF_6:Mn^{4+}) formed. The phosphor was collected and washed with acetone several times to remove residues and then dried for several hours in an oven at 110 °C.

2.2.3. Procedure for conversion from Rb_2SiF_6:Mn^{4+} to Rb_2KSiF_7:Mn^{4+} (step 2 in Fig. 1). Rb_2KSiF_7:Mn^{4+} was synthesized *via* a solid-state reaction method. The prepared Rb_2SiF_6:Mn^{4+} phosphor and various ratios of KHF_2 were mixed an agate mortar until a homogeneous mixture was obtained. The mixed powder was sintered in a BN crucible at 300 °C for several hours under N_2/H_2 mixture gas (N_2 gas: 100–75%, H_2 gas: 0–25%, flow rate: 600 cm^3 min^{-1}) in a horizontal tube furnace. The products were cooled to room temperature, ground, and then washed with ethanol several times to remove the remaining substances and to prevent aggregation.

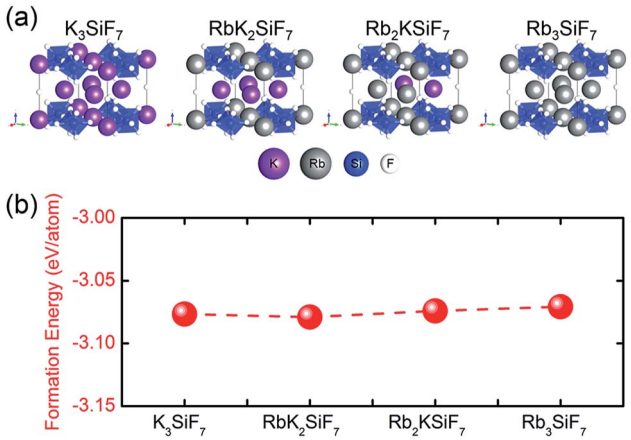

Fig. 2 (a) Atomic geometries of $Rb_xK_{3-x}SiF_7$. The violet, pink, blue, and white balls represent K, Rb, Si, and F atoms, respectively. (b) Bulk formation energies of the $Rb_xK_{3-x}SiF_7$ structures.

2.3. Characterization

The crystal structures of the phosphors (Rb_2KSiF_7:Mn^{4+}) were determined by X-ray diffraction (XRD, Rigaku D/Max 220V) using Cu K_α radiation (Ni filter, voltage: 40 kV, current: 40 mA), as shown in Fig. 1(c). To investigate the morphology and the size of the prepared phosphors, we used scanning electron microscopy (SEM; JEOL JSM-6360). The composition of the samples was analyzed by energy-dispersive X-ray spectrometry (EDS) using a spectrometer (Bruker Quantax 200) with an energy resolution <127 eV (HV: 20.0 kV). The optical characteristics of the phosphors were examined at room temperature using a photoluminescence spectrometer (DARSA PRO-5000) and a Xe light source (500 W). Thermogravimetric analysis (TGA) and differential thermal analysis (DTA) of the phosphors were conducted on a Thermo Plus EVO II (TG8120 series, DSC 8230) at a heating rate of 5 °C min^{-1} under flowing N_2 gas.

3. Results and discussion

Fig. 2(a) shows the atomic geometries of the $Rb_xK_{3-x}SiF_7$ structures. With increasing x in $Rb_xK_{3-x}SiF_7$, the lattice parameters and cell volume increase, as shown in Table 1, because the atomic radius of Rb (2.35 Å) is slightly larger than that of K (2.20 Å).[15] The trend of the calculated lattice parameters with increasing Rb content is consistent with the trend of the experimental lattice parameters.[16,17] In particular, in the cases of binary cations (Rb^+ and K^+), various structural configurations in which Rb^+ or K^+ ions occupy positions in the unit cell are possible (see Fig. S1 in ESI†). The RbK_2SiF_7 and Rb_2KSiF_7 atomic geometries shown in Fig. 2(a) were chosen as the structures with the most stable total energy among the various investigated configurations. These two energetically preferred structures exhibit interesting structural features. The RbK_2SiF_7 and Rb_2KSiF_7 atomic geometries include K-2D-layer (green trapezium) and K-1D-chain (red arrow) substructures within their atomic structures, respectively (see Fig. S2 in ESI†). We speculated that such substructures energetically stabilize their associated atomic structures.

Table 1 Experimental and theoretical lattice parameters for $Rb_xK_{3-x}SiF_7$

Tetragonal ($P4/mbm$)	Experiment			Theory (this work)		
	a (Å)	b (Å)	c (Å)	a (Å)	b (Å)	c (Å)
K_3SiF_7	7.74	7.74	5.56	7.87	7.87	5.64
RbK_2SiF_7				7.94	7.94	5.72
Rb_2KSiF_7	7.88	7.88	5.72	8.04	8.04	5.82
Rb_3SiF_7	7.95	7.95	5.82	8.14	8.14	5.92

In addition, we calculated the bulk formation energies of the $Rb_xK_{3-x}SiF_7$ structures. The formation energy, ΔH_f, for $Rb_xK_{3-x}SiF_7$ is given by $\Delta H_f = E_{tot} - \sum_i \mu_i x_i$, where E_{tot} is the total energy of the structure, μ_i is the chemical potential of element i, and x_i is the number of elements i in the structure.[18] In terms of the design of a new host material for conversion phosphors, the DFT formation energy can be an important indicator for determining whether a phosphor material can be synthesized. As shown in Fig. 2(b), all of the $Rb_xK_{3-x}SiF_7$ structures have negative formation energies, which indicates that all of the structures we considered can be synthesized. Among these compounds, all except Rb_2KSiF_7 have been reported experimentally.[16,17]

Furthermore, we calculated the energy band structures and DOSs of the $Rb_xK_{3-x}SiF_7$ system (see Fig. S3 in ESI†). With increasing Rb content, the bandgap of the host material system decreases from 5.59 eV to 5.33 eV. This decrease of the bandgap energy is related to the increase of the lattice parameters with increasing Rb content. Because of the large radius of Rb atoms, an increase of the Rb content (with Rb substitution at the K sites) leads to an expansion of the $Rb_xK_{3-x}SiF_7$ unit-cell volume. Accordingly, the increase of the cell volume leads to weakening of the binding forces of the atoms' valence electrons. Consequently, the valence electrons become freer with increasing interatomic distance, which eventually reduces the bandgap which corresponds to the energy required for valence electrons to be promoted to the conduction band (CB).

From the atomic projected DOSs, we find that, although the CB is derived mainly from the Rb d state, the F p state contributes to the upper valence band (VB) (see Fig. S4 in ESI†). An enlarged image of the CB region from 5 eV to 10 eV is shown in the inset of each DOS diagram. As the Rb content increases, the Rb d state (in the CB) and Rb p state (near −8 eV, marked with a blue star) are enhanced. These Rb-related DOSs do not appear to strongly affect the F- or Si-related states.

One of the important factors in the development of conversion red phosphors is their emission wavelength. If the emission wavelength of the candidate material can be predicted before the material is actually synthesized, the phosphor development time would be dramatically reduced, leading to the efficient design of effective phosphor materials. Consequently, the ability to predict the emission energy of the doping system is important. For Mn-doped phosphor systems, the

emission light is known to originate from the spin-flip transition of Mn^{4+}, such as the transition from the ^2E_g excited state to the $^4A_{2g}$ ground state. As shown in Fig. 3(a), low-spin (1 μ_B) and high-spin (3 μ_B) states correspond to the ^2E_g excited state and the $^4A_{2g}$ ground state, respectively.[19] Therefore, the emission energy of Mn^{4+} can be predicted by calculating the total energy difference between the low-spin state and the high-spin state. The emission energy was calculated according to the equation Emission Energy $= E_{\text{low-spin}} - E_{\text{high-spin}}$, where $E_{\text{low-spin}}$ and $E_{\text{high-spin}}$ are the total energies of Mn^{4+} doped systems with relaxed low-spin (1 μ_B) and high-spin (3 μ_B) states, respectively.

To calculate emission energies that account for the effects of Mn doping on the four $Rb_xK_{3-x}SiF_7$ ($x = 0, 1, 2, 3$) host materials, we first calculated the atomic and electronic structures of Mn-doped $Rb_xK_{3-x}SiF_7$. Fig. 3(b) shows the atomic geometry of the $Rb_2KSi_{0.75}Mn_{0.25}F_7$ structure. To minimize the effect of Mn–Mn interaction on the electronic structure, we introduced a $1 \times 1 \times 2$ super cell structure. Among four Si sites (Si_1, Si_2, Si_3, and Si_4 sites), a Si atom was replaced with a Mn atom and the minimum Mn–Mn interatomic distance was 7.8 Å. Fig. S5 in ESI† shows the atomic projected DOSs on the $^4A_{2g}$ ground (left side) and ^2E_g excited (right side) states of the $Rb_xK_{3-x}SiF_7:Mn^{4+}$ structures. In all of the DOSs, both the t_{2g} and e_g states of Mn atoms are hybridized with the F p states. That is, the t_{2g} and e_g states between the bandgap of the host are donated by the Mn 3d and the F 2p orbitals. In addition, the $^4A_{2g}$ ground and ^2E_g excited states have high-spin (3 μ_B) and low-spin (1 μ_B) configurations, respectively. In particular, in the ^2E_g excited state, a small Jahn–Teller distortion will eventually manifest as splitting of the t_{2g} and e_g states, as shown in the right side of Fig. S5 in ESI†.[19] These DOS results are similar to those reported in a previous study.[19] No particular trend of the mid-gap states (t_{2g} and e_g states) with respect to the Rb content was found.

From the total energies of the ground states, we also calculated the formation energies for substitution of Mn at the Si site in $Rb_xK_{3-x}SiF_7$. The formation energy for Mn substitution, $E^{\text{form}}_{\text{Mn-sub}}$, was calculated to assess the ease with which a Mn atom can replace a Si atom in a certain host material. It was calculated according to the equation $E^{\text{form}}_{\text{Mn-sub}} = E_{\text{Mn:RKSF}} + \mu_{\text{Si}} - (E_{\text{RKSF}} + \mu_{\text{Mn}})$, where $E_{\text{Mn:RKSF}}$ is the total energy of the ground state of $Rb_xK_{3-x}SiF_7:Mn^{4+}$, E_{RKSF} is the total energy of undoped $Rb_xK_{3-x}SiF_7$, μ_{Si} is the total energy per atom of bulk Si, and μ_{Mn} is the total energy per atom of bulk Mn. As shown in Fig. 3(c), as the Rb content increases, the formation energy for Mn substitution decreases. This trend is attributed to the lattice expansion induced by the Rb substitution promoting Mn doping (at Si sites).

The results in Fig. 3(d) confirm that the simulated emission energy value fluctuates irrespective of the Rb content. Notably, the $Rb_2KSiF_7:Mn^{4+}$ exhibits the longest simulated emission wavelength among the $Rb_xK_{3-x}SiF_7:Mn^{4+}$ phosphors. On the basis of this result, we expected the light emission from $Rb_2KSiF_7:Mn^{4+}$ to shift toward longer emission wavelengths compared with the wavelengths of the emissions from $K_3SiF_7:Mn^{4+}$. In terms of material design of a new conversion phosphor, the aforementioned results provide an important guideline for the synthesis of host materials.

On the basis of the material insights gained thus far through theoretical investigations, we attempted to synthesize a new red conversion phosphor corresponding to Mn-doped $Rb_xK_{3-x}SiF_7$ ($x > 1$) using various methods. As a result, we obtained three phosphors: $K_3SiF_7:Mn^{4+}$, $Rb_3SiF_7:Mn^{4+}$ and $Rb_2KSiF_7:Mn^{4+}$. The $K_3SiF_7:Mn^{4+}$ phosphor has already been reported.[8] Thus, we successfully synthesized two new conversion red phosphors, $Rb_3SiF_7:Mn^{4+}$ and $Rb_2KSiF_7:Mn^{4+}$, with a host material containing Rb. For reference, $RbK_2SiF_7:Mn^{4+}$, which has not been reported in the ICSD database, was also not obtained in the present study. In addition, $Rb_3SiF_7:Mn^{4+}$, which we successfully synthesized, was very unstable, exhibiting sensitivity to moisture; it structure fragmented soon after it was synthesized. However, the $Rb_2KSiF_7:Mn^{4+}$ red phosphor exhibited very stable structural characteristics.

The procedure for the synthesis of $Rb_2KSiF_7:Mn^{4+}$ is detailed in Fig. 1(a) and (b) and in Section 2.2. The crystallographic data (see Table S1 in ESI†) determined from Rietveld refinement with XRD patterns of the synthesized $Rb_2KSiF_7:Mn^{4+}$, as the first conclusive evidence of the successful synthesis of $Rb_2KSiF_7:Mn^{4+}$, shows good agreement with the reported experimental lattice parameters for Rb_2KSiF_7 in Table 1.[16,17]

Fig. 4(a) shows the normalized PL (λ_{ex} = 460 nm) and photoluminescence excitation (PLE) (λ_{em} = 630 nm) spectra of the $K_2SiF_6:Mn^{4+}$, $K_3SiF_7:Mn^{4+}$ and $Rb_2KSiF_7:Mn^{4+}$ phosphors.

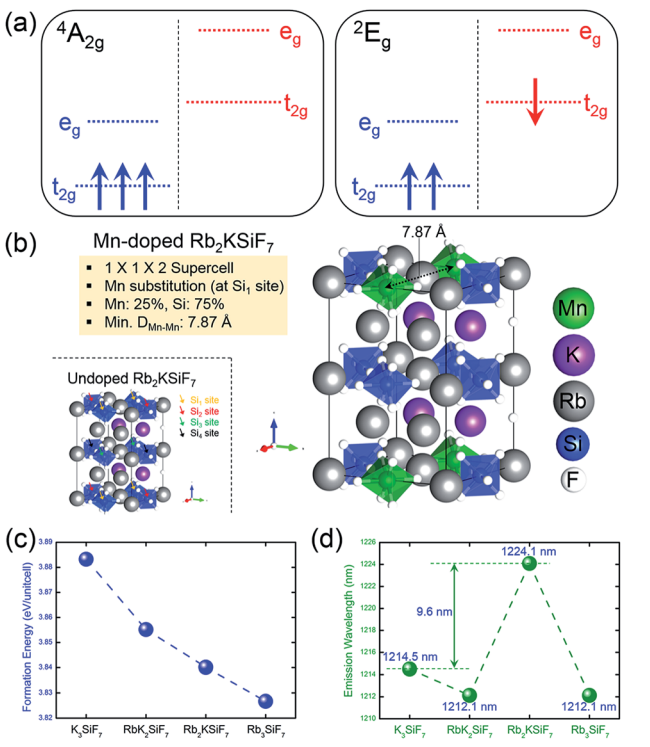

Fig. 3 (a) Schematic energy diagrams of the $^4A_{2g}$ ground state and ^2E_g excited state of Mn^{4+}. (b) Atomic geometries of Rb_2KSiF_7 (undoped) and $Rb_2KSi_{0.75}Mn_{0.25}F_7$ (Mn-doped) structures. The green, violet, pink, blue, and white balls represent Mn, K, Rb, Si, and F atoms, respectively. (c) Formation energies of $Rb_xK_{3-x}SiF_7:Mn^{4+}$ with Mn substituted at Si sites and (d) the simulated emission wavelengths of the Mn-substituted products.

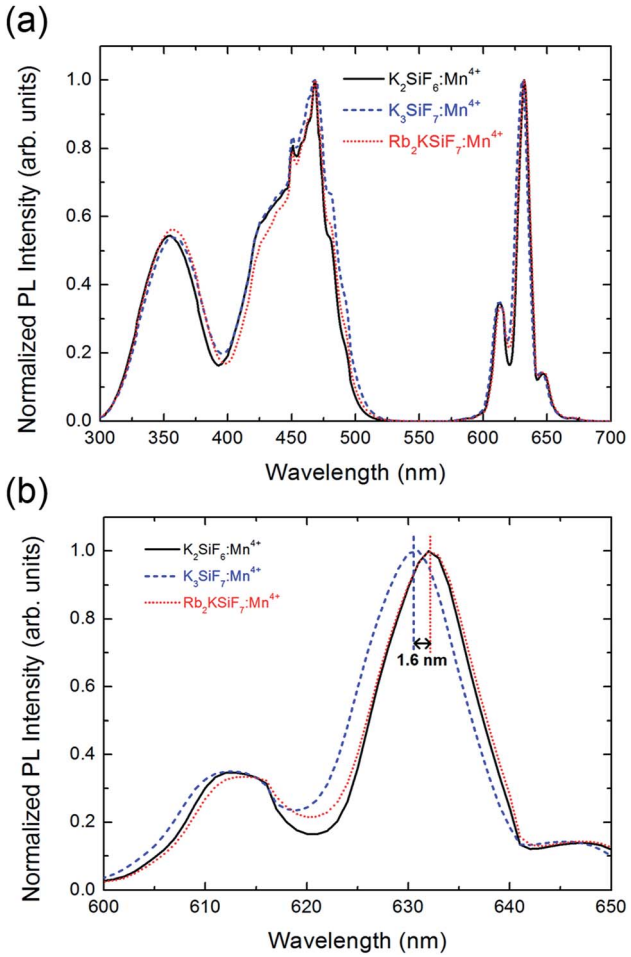

Fig. 4 (a) Normalized PL (λ_{ex} = 460 nm) and PLE (λ_{em} = 630 nm) spectra of $K_2SiF_6:Mn^{4+}$, $K_3SiF_7:Mn^{4+}$, and $Rb_2KSiF_7:Mn^{4+}$ phosphors. (b) An enlargement of the PL spectra in the wavelength range from 600 nm to 650 nm.

As shown in the right side of the Fig. 4(a), all three phosphors not only show very strong and narrow red luminescence in the wavelength region near 630 nm but also show very stable excitation from 330 nm to 480 nm. To examine the PL results more closely, the spectral region from 600 nm to 650 nm was enlarged (Fig. 4(b)). Here, $Rb_2KSiF_7:Mn^{4+}$ clearly emits longer-wavelength light than $K_3SiF_7:Mn^{4+}$ and has an emission wavelength almost equal to that of $K_2SiF_6:Mn^{4+}$. Furthermore, the PL efficiency of $Rb_2KSiF_7:Mn^{4+}$ sample (having the highest PL) corresponds to 85% of that of $K_2SiF_6:Mn^{4+}$ (93% of that of $K_3SiF_7:Mn^{4+}$), as shown in Fig. S6 in ESI.† These results indicate that luminescence with an emission wavelength similar to that of the conventional $K_2SiF_6:Mn^{4+}$ phosphor can be induced from a Rb-containing quaternary fluoride phosphor. It also shows good agreement with the theoretical calculation results indicating that the simulated emission wavelength of $Rb_2KSiF_7:Mn^{4+}$ is the longest among the investigated phosphors (Fig. 3(d)); thus, such calculation results can provide rational insights into the properties of a phosphor material before it is synthesized.

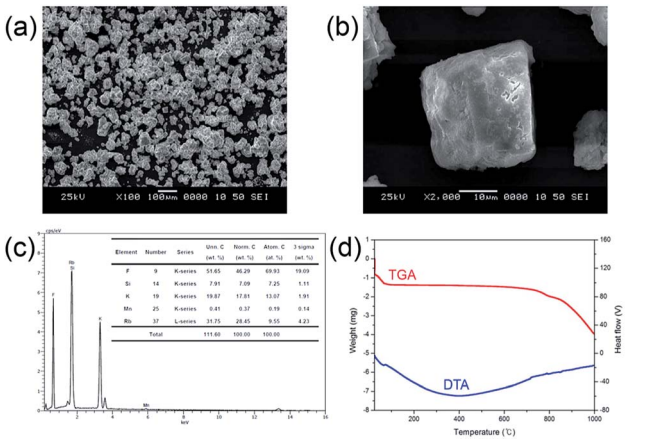

Fig. 5 (a) and (b) SEM images, (c) EDS diagram, and (d) TGA and DTA curves of the $Rb_2KSiF_7:Mn^{4+}$ phosphor.

Particle morphology is a key factor for phosphor materials used in white LEDs. It is influenced by various physico-chemical parameters such as sintering temperature, holding time, precursor materials, chemical composition, crystal structure, and homogeneity, especially when the powders are produced by the solution process *via* amorphous precursor particles. The morphologies of the particles of the synthesized phosphor materials were observed by SEM. Fig. 5(a) and (b) show the morphology of the Mn^{4+}-doped Rb_2KSiF_7 powder. Particles with various sizes (approximately 50–100 μm) and shape distributions are observed to be dispersed as shown in Fig. 5(a). In assessing the suitability of the red conversion phosphor for use in white LEDs, not only its morphological properties but also its thermal characteristics should be considered. Fig. 5(d) displays the TGA and DTA curves of the $Rb_2KSiF_7:Mn^{4+}$ phosphor. The TGA result shows over two the steps weight drops at around 700 °C and 800 °C. Moreover, DTA exhibits two DTA peaks at 710 °C and 790 °C. These results indicate that the $Rb_2KSiF_7:Mn^{4+}$ phosphor is not only decomposed over the two steps into SiF_4 and alkali metal fluorides (RbF or KF) but also thermally stable to 750 °C.[20] Apart from thermal stability of phosphor structure, we checked the temperature-dependent PL properties of $Rb_2KSiF_7:Mn^{4+}$ (see Fig. S7 in ESI†). As a results, the luminescent property of $Rb_2KSiF_7:Mn^{4+}$ phosphor exhibits thermally stable properties up to 125 °C, but, above 150 °C, PL quenching occurs rapidly. Even if the temperature was lowered again, PL intensity degraded by high temperature was not recovered.

4. Conclusions

We performed first-principles calculations based on DFT for pristine and Mn-doped $Rb_xK_{3-x}SiF_7$ (x = 0, 1, 2, 3) and predicted their stability, electronic structure, and luminescence properties. According to the results of calculations for the $Rb_xK_{3-x}SiF_7$ (x = 0, 1, 2, 3) host structures performed prior to the calculation for the Mn-doped system, all of the compounds

exhibit a large negative bulk formation energy, which indicates that all of the structures considered in this study could be synthesized. Moreover, as the content of Rb increases in the $Rb_xK_{3-x}SiF_7$ host system, their bandgap energy decreases from 5.59 eV to 5.33 eV. From the atomic projected DOSs, we found that, while the CB is derived mainly form the Rb d state, the upper VB arises from the F p state. For the Mn-doped $Rb_xK_{3-x}SiF_7$ phosphor system, we calculated the formation energy for Mn substitution and the simulated emission energy of each structure. As a result, we found that, with increasing Rb content, the formation energy for Mn substitution decreases. This trend was attributed to the Rb substitution expanding the lattice because of larger size of Rb ion than K ion. The lattice expanding could promote Mn doping at Si sites.

On the basis of the knowledge gained through the simulations, we next synthesized red conversion phosphors and investigated their luminescence, structure, and stability. As a result, we successfully prepared the stable new red conversion phosphor $Rb_2KSiF_7:Mn^{4+}$. In addition, the $Rb_2KSiF_7:Mn^{4+}$ emitted at a longer wavelength than the $K_3SiF_7:Mn^{4+}$ and exhibited an emission wavelength similar to that of $K_2SiF_6:Mn^{4+}$. This similarity indicated that a red phosphor with a luminescence wavelength similar to that of the conventional $K_2SiF_6:Mn^{4+}$ phosphor was prepared as a quaternary fluoride phosphor containing Rb. It also showed good agreement with our theoretical calculation results, which shows that $Rb_2KSiF_7:Mn^{4+}$ exhibited the longest simulated emission wavelength among the four Mn-doped structures.

Collectively, these results demonstrate that DFT calculations can provide rational insights into the properties of a red phosphor material before it is synthesized, thereby reducing the time and cost required to develop new red conversion phosphors.

Conflicts of interest

There are no conflicts to declare.

Acknowledgements

This research was supported by the Nano Material Technology Development Program through the National Research Foundation of Korea funded by the Ministry of Science and ICT (NRF-2016M3A7B4025408).

Notes and references

1 Y. H. Kim, P. Arunkumar, B. Y. Kim, S. Unithrattil, E. Kim, S.-H. Moon, J. Y. Hyun, K. H. Kim, D. Lee, J.-S. Lee and W. B. Im, *Nature*, 2017, **16**, 543–550.
2 M. Zhao, H. Liao, L. Ning, Q. Zhang, Q. Liu and Z. Xia, *Adv. Mater.*, 2018, **30**, 1802489.
3 S. Liang, M. Shang, H. Lian, K. Li, Y. Zhang and J. Lin, *J. Mater. Chem. C*, 2017, **5**, 2927–2935.
4 X. Piao, K.-I. Machida, T. Horikawa, H. Hanzawa, Y. Shimomura and N. Kijima, *Chem. Mater.*, 2007, **19**, 4592–4599.
5 S. Jang, J. Im, B. K. Bang, C. H. Kim, H. Chang and K.-J. Kong, *RSC Adv.*, 2015, **5**, 39319–39323.
6 T. Takahashi and S. Adachi, *J. Electrochem. Soc.*, 2008, **155**, E183–E188.
7 H. F. Sijbom, R. Verstraete, J. J. Joos, D. Poelman and P. F. Smet, *Opt. Mater. Express*, 2017, **7**, 3332–3365.
8 M. Kim, W. B. Park, B. Bang, C. H. Kim and K.-S. Sohn, *J. Am. Ceram. Soc.*, 2017, **100**, 1044–1050.
9 Y. Zhuo, A. M. Tehrani, A. O. Oliynyk, A. C. Duke and J. Brgoch, *Nat. Commun.*, 2018, **9**, 4377.
10 C. H. Kim, B. K. Bang, J. K. Park, K.-J. Kong, H. Chang, J. Im, S. Jang and K. S. Choi, KR 101790541, 2017.
11 G. Kresse and J. Furthmüller, *Phys. Rev. B: Condens. Matter Mater. Phys.*, 1996, **54**, 11169–11186.
12 G. Kresse and J. Hafner, *Phys. Rev. B: Condens. Matter Mater. Phys.*, 1993, **47**, 558–561.
13 J. P. Perdew, K. Burke and M. Ernzerhof, *Phys. Rev. Lett.*, 1996, **77**, 3865–3868.
14 P. E. Blochl, *Phys. Rev. B: Condens. Matter Mater. Phys.*, 1994, **50**, 17953–17979.
15 J. C. Slater, *J. Chem. Phys.*, 1964, **41**, 3199.
16 D. L. Deadmore and W. F. Bradley, *Acta Crystallogr.*, 1962, **15**, 186–189.
17 B. Hofmann and R. Hoppe, *Z. Anorg. Allg. Chem.*, 1979, **458**, 151–162.
18 S. Kirklin, J. E Saal, B. Meredig, A. Thompson, J. W. Doak, M. Aykol, S. Rühl and C. Wolverton, *npj Comput. Mater.*, 2015, **1**, 15010.
19 M. H. Du, *J. Mater. Chem. C*, 2014, **2**, 2475–2481.
20 R. Verstraete, H. F. Sijbom, J. J. Joos, K. Korthout, D. Poelman, C. Detavernier and P. F. Smet, *ACS Appl. Mater. Interfaces*, 2018, **10**, 18845–18856.